Tactile-based Blind Grasping: A Discrete-Time Object Manipulation Controller for Robotic Hands

Wenceslao Shaw-Cortez[1], Denny Oetomo[1], Chris Manzie[1], and Peter Choong[2]

***Abstract*—Robust object manipulation using a robotic hand remains a challenging task, especially when a priori knowledge of the object being manipulated is not available. Tactile-based blind grasping is hereby defined where only typical sensors on-board the robotic hand unit are available. In this paper we propose a robust discrete-time controller for tactile-based blind grasping to manipulate unknown objects. The analysis contained herein shows that from an initial stable pose, tactile feedback in the form of contact location and joint measurements are sufficient information to perform object manipulation, and ensure that the object does not slip. Furthermore, the analysis guarantees semi-global practical asymptotic stability of the closed loop system, and takes into consideration the effect of sampling time. The robustness of the proposed control is demonstrated through simulation and experiments.**

***Index Terms*—Dexterous Manipulation, Multifingered Hands, Robust/Adaptive Control of Robotic Systems**

I. Introduction

ROBOTICS research has addressed object manipulation heavily in the past few decades, but existing solutions have yet to translate into real-world scenarios where the robotic hand has limited knowledge of the environment. The early literature assumes perfect knowledge of grasp properties including object center of mass, object mass, external wrench, and contact friction [1], [2]. However when a robotic hand is deployed in the real world, it is impractical to assume a priori knowledge of all grasp properties. Powered prosthetic hands, for example, are generally restricted to on-board sensing due to the low information transfer in the human-machine interface, and thus have no a priori information of the object to be grasped [3].

Tactile-based blind grasping, as defined here, consists of a robotic hand grasping/manipulating an object with no external sources of information including knowledge of the object center of mass, object mass, coefficient of friction, and external wrench disturbances. The robotic hand only has access to on-board sensors that can be integrated into the robotic hand. Acceptable sensors include tactile sensors that are regarded as an intuitive and practical means of gathering information for grasping/manipulation tasks.

The difficulty in providing object manipulation for tactile-based blind grasping resides in dealing with the uncertainties of the grasp, while ensuring that the object does not slip. In [4] a robust PD control law with adaptive compensation was proposed, but does not guarantee slipping is avoided. In [5], a passivity-based controller without tactile sensing was developed, but is not robust to unknown external disturbances. In [6], [7] impedance-based controllers were presented/compared, but do not guarantee the object will not slip. One important feature of the related literature is the use of an approximate object frame defined with respect to the hand configuration to provide a reference for manipulation. This task frame is used as a result of the lack of knowledge of the object motion in tactile-based blind grasping [5]–[7].

In addition to robustness in the manipulation controller, it is important to satisfy friction constraints such that the object does not slip out of the grasp during a manipulation motion [1], [2]. However, much of the related literature does not guarantee that the object will not slip [4]–[7], and instead, heuristically grasp the object by directing the fingertips towards the centroid of the grasp. That approach is likely to fail in cases where the projected squeezing forces create large shear forces along the contact surface, which causes slipping. Figure 1 shows an example of how that grasping approach induces slip and compromises the stability of the system during manipulation.

(a) Initial grasp (b) Unstable grasp

Fig. 1: Conventional control resulting in slipping and instability during manipulation. Red arrows indicate the contact forces exerted by the fingertips towards the grasp centroid.

Grasp force optimization is a technique that exploits grasp redundancy for improved grasp performance and to prevent slip. In the conventional literature, that technique uses knowledge of the grasp properties such as object center of mass, mass, contact location, friction coefficient, and external wrench to ensure the object does not slip, while minimizing a cost, such as actuator torques [8]–[10]. Those approaches are invalid in tactile-based blind grasping due to the use of exter-

Manuscript received: September, 10, 2017; Revised December, 12, 2017; Accepted January, 7, 2018.

This paper was recommended for publication by Editor Han Ding upon evaluation of the Associate Editor and Reviewers' comments. This work was supported by the Valma Angliss Trust.

[1]W. Shaw-Cortez, D. Oetomo, and C. Manzie are with the MIDAS Laboratory in the School of Electrical, Mechanical, and Infrastructure Engineering, University of Melbourne, 3010, Australia shaww@student.unimelb.edu.au, {doetomo,manziec}@unimelb.edu.au

[2]Peter Choong is with the Department of Surgery, University of Melbourne, St. Vincent's Hospital, 3065, Australia pchoong@unimelb.edu.au

Digital Object Identifier (DOI): see top of this page.

nal information. Furthermore, those optimization-in-the-loop approaches exploit the discrete-time nature of commanding robotic hands, but do not consider the effects of sampling time with the system dynamics. Without analysis of inter-sampling behavior, those approaches can not guarantee stability of the closed loop system and thus may result in grasping instabilities. One exceptional technique is robust to uncertainties in the contact locations and object information [11], but is limited to static grasps. Other exceptional approaches combine a robust manipulation controller with grasp force optimization, but require knowledge of the object center of mass, assume the contact points do not roll, and ignore the effects of sampling time [12], [13].

In previous work, we proposed a manipulation controller that is robust to uncertainties in the object center of mass, object mass, hand kinematics, contact locations, and external wrenches under rolling effects, but required the assumption that the object does not slip [14]. We extend that work here by incorporating existing tactile sensors that can be physically self-contained into the robotic hand [15]. The proposed control integrates the tactile information with the robust controller from [14] using a robust form of grasp force optimization to relax the no slip assumption. The analysis herein shows how the no slip assumption is relaxed, while also considering the effect of sampling time on the system. The proposed controller is implemented in simulation and experiment for validation.

Notation: Throughout this paper, the index i is specifically used to index over the n contact points in the grasp. An indexed vector $\boldsymbol{v}_i \in \mathbb{R}^p$ has an associated concatenated vector $\boldsymbol{v} \in \mathbb{R}^{pn}$. The index k is used to indicate the sampling instant in time such that for a time-dependent variable $\boldsymbol{v}(t)$, $\boldsymbol{v}_k := \boldsymbol{v}(t = kT_s)$ where $T_s \in \mathbb{R}_{>0}$ is the sampling time. The notation $\boldsymbol{v}^{\mathcal{E}}$ indicates that the vector $\boldsymbol{v}$ is written with respect to a frame $\mathcal{E}$, and if there is no explicit frame defined, $\boldsymbol{v}$ is written with respect to the inertial frame, $\mathcal{P}$. $SO(3)$ denotes the special orthogonal group of dimension 3. The operator $(\cdot)\times$ denotes the skew-symmetric matrix representation of the cross-product. The centroid of the vector $\boldsymbol{v} \in \mathbb{R}^{pn}$ is defined by $\bar{\boldsymbol{v}} = \frac{1}{n}\sum_{i=1}^{n} \boldsymbol{v}_i$. The kernel or null-space of a matrix, B, is denoted by $\text{Ker}(B)$. The Moore-Penrose generalized inverse of B is denoted $B^{\dagger}$. The $n\times n$ identity matrix is denoted $I_{n\times n}$.

II. Problem Formulation

A. System Model

Consider a fully-actuated, multi-fingered hand grasping a rigid, convex object at n contact points. The grasp consists of one contact point per finger with smooth, convex fingertips of high stiffness that each apply a contact force, $\boldsymbol{f}_{c_i} \in \mathbb{R}^3$, on the object. Let the hand configuration be defined by the joint angles, $\boldsymbol{q} \in \mathbb{R}^m$. Let the inertial frame, $\mathcal{P}$, be fixed on the palm of the hand, and a fingertip base frame, $\mathcal{F}_i$, fixed at the point $\boldsymbol{p}_{f_i} \in \mathbb{R}^3$. The contact frame, $\mathcal{C}_i$, is located at the contact point, $\boldsymbol{p}_{c_i} \in \mathbb{R}^3$. The position vector from $\mathcal{F}_i$ to $\mathcal{C}_i$ is $\boldsymbol{p}_{fc_i} \in \mathbb{R}^3$. The position vector from $\mathcal{F}_i$ to an arbitrary point fixed on the fingertip is denoted $\boldsymbol{p}_{ft_i} \in \mathbb{R}^3$. Without loss of generality, $\boldsymbol{p}_{ft_i}$ is fixed at the center of the fingertip. The inertial position of this fixed point is $\boldsymbol{p}_{t_i}(\boldsymbol{q}) = \boldsymbol{p}_{f_i}(\boldsymbol{q}) + \boldsymbol{p}_{ft_i}$.

A visual representation of the contact geometry for the ith finger is shown in Figure 2.

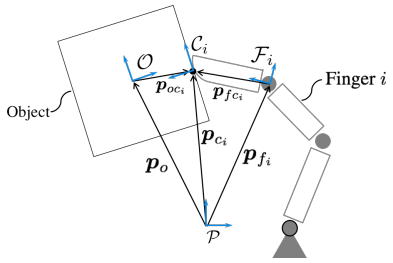

Fig. 2: A visual representation of the contact geometry for contact i.

Let $\mathcal{O}$ be a reference frame fixed at the object center of mass $\boldsymbol{p}_o \in \mathbb{R}^3$, and $R_{po} \in SO(3)$ is the rotation matrix, which maps from $\mathcal{O}$ to $\mathcal{P}$. The object pose is defined by $\boldsymbol{x}_o \in \mathbb{R}^6$. The position vector from the object center of mass to the respective contact point is $\boldsymbol{p}_{oc_i} \in \mathbb{R}^3$.

To ensure slip does not occur, each contact force must remain inside the friction cone defined by:

$$F_{c_i} = \{\boldsymbol{f}_{c_i}^{\mathcal{C}_i} \in \mathbb{R}^3 : f_{n_i}\mu \geq \sqrt{f_{x_i}^2 + f_{y_i}^2}\} \tag{1}$$

where $\boldsymbol{f}_{c_i}^{\mathcal{C}_i} = (f_{x_i}, f_{y_i}, f_{n_i})$ is the contact force at i written in frame $\mathcal{C}_i$ with tangential force components $f_{x_i}, f_{y_i} \in \mathbb{R}$ and normal force component $f_{n_i} \in \mathbb{R}$, and $\mu \in \mathbb{R}_{>0}$ is the friction coefficient. The full friction cone is the Cartesian product of all the friction cones: $F_c = F_{c_1} \times ... \times F_{c_n}$.

Conventionally, a manipulation task is described by the translation/rotation of a coordinate frame fixed to the object center of mass [2]. However in tactile-based blind grasping, the object center of mass is unknown and so a task frame must be defined with respect to the available on-board sensors. Let $\mathcal{A}$ be the task frame located at the point $\boldsymbol{p}_a \in \mathbb{R}^3$ with respect to $\mathcal{P}$. Let $R_{pa} \in SO(3)$ be the rotation matrix mapping from frame $\mathcal{A}$ to $\mathcal{P}$. Let $\boldsymbol{\omega}_a \in \mathbb{R}^3$ denote the angular velocity of frame $\mathcal{A}$ with respect to $\mathcal{P}$. The task frame state $\boldsymbol{x} \in \mathbb{R}^6$ is defined by the position $\boldsymbol{p}_a$ and orientation of the task frame.

The hand-object dynamics are respectively defined as [16]:

$$M_h\ddot{\boldsymbol{q}} + C_h\dot{\boldsymbol{q}} = -J_h^T\boldsymbol{f}_c + \boldsymbol{\tau}_e + \boldsymbol{u} \tag{2}$$

$$M_o\ddot{\boldsymbol{x}}_o + C_o\dot{\boldsymbol{x}}_o = G\boldsymbol{f}_c + \boldsymbol{w}_e \tag{3}$$

where $M_h := M_h(\boldsymbol{q}) \in \mathbb{R}^{m\times m}$, $M_o := M_o(\boldsymbol{x}_o) \in \mathbb{R}^{6\times 6}$ are the respective hand and object inertia matrices, $C_h := C_h(\boldsymbol{q}, \dot{\boldsymbol{q}}) \in \mathbb{R}^{m\times m}$, $C_o := C_o(\boldsymbol{x}_o, \dot{\boldsymbol{x}}_o) \in \mathbb{R}^{6\times 6}$ are the respective hand and object Coriolis and centrifugal matrices, $\boldsymbol{\tau}_e := \boldsymbol{\tau}_e(t, \boldsymbol{q}, \dot{\boldsymbol{q}}) \in \mathbb{R}^m$ is the sum of all dissipative and non-dissipative disturbance torques acting on the joints, $\boldsymbol{w}_e := \boldsymbol{w}_e(t) \in \mathbb{R}^6$ is an external wrench disturbing the object, and $\boldsymbol{u} \in \mathbb{R}^m$ is the joint torque control input for a fully actuated hand. The disturbance, $\boldsymbol{\tau}_e$, contains the disturbance torque caused by gravity, which we specifically denote as $\boldsymbol{g} := \boldsymbol{g}(\boldsymbol{q}, \boldsymbol{n}_g) \in \mathbb{R}^m$, where $\boldsymbol{n}_g \in \mathbb{R}^3$ is the unit vector oriented in the direction of gravity with respect to $\mathcal{P}$. The grasp map, $G := G(\boldsymbol{p}_{oc}) \in \mathbb{R}^{6\times 3n}$ maps the contact force, $\boldsymbol{f}_c$, to the net wrench acting on the object. The hand Jacobian, $J_h := J_h(\boldsymbol{q}, \boldsymbol{p}_{fc}) \in \mathbb{R}^{3n\times m}$, relates the motion of the hand and velocity of the contact points.

The following assumptions are made for the grasp:

Assumption 1. *The given hand has sufficient degrees of freedom such that $m = 3n$, and never reaches a singular configuration.*

Assumption 2. *The given multi-fingered grasp has $n > 2$ non-collinear contact points.*

Assumption 3. *The hand is equipped with sensors that provide measurements of the joint angles, $\boldsymbol{q}$, contact locations $\boldsymbol{p}_{fc}$, and the gravity direction vector $\boldsymbol{n}_g$.*

Assumption 4. *The intersection of Ker(G) and F_c is never empty, and $\boldsymbol{f}_c(0) \in F_c$.*

Assumption 5. *The fingertip and object surfaces at the contact points are locally smooth.*

Remark 1. *Assumption 1 ensures J_h is square and invertible, which is a common assumption in related work [5], [6], [12], and can be relaxed by considering internal motion of the dynamics [16]. Assumption 2 ensures G is always full rank [2]. Assumption 4 ensures that under the given grasp, the hand is capable of holding the object, and that the object is not slipping initially. Assumptions 2 and 4 can be satisfied by existing grasp formation planners [17].*

Many existing solutions assume the disturbances $\boldsymbol{\tau}_e, \boldsymbol{w}_e$ to be zero, or exactly known so as to simply be canceled out [2], [5], [12]. Here we relax that assumption by allowing for unknown disturbances that are constant at the origin:

Assumption 6. *The disturbances, $\boldsymbol{\tau}_e, \boldsymbol{w}_e$, are continuously differentiable, bounded, and satisfy: $(\dot{\boldsymbol{x}}, \ddot{\boldsymbol{x}}) = 0 \implies \dot{\boldsymbol{\tau}}_e, \dot{\boldsymbol{w}}_e = 0$.*

Common disturbances that satisfy Assumption 6 include gravity acting on both the hand and object, and viscous friction acting on the joints [14].

B. Control Objective

Let $\boldsymbol{r} \in \mathbb{R}^6$ be the reference command that defines the desired pose of the task frame A, and let $\boldsymbol{e} = \boldsymbol{x} - \boldsymbol{r}$ define the error state. In this paper we focus on set-point manipulation such that the reference is piece-wise constant and $\dot{\boldsymbol{r}}, \ddot{\boldsymbol{r}} \equiv 0$. For object manipulation, the goal is to translate/rotate A to the reference such that $(\boldsymbol{e}, \dot{\boldsymbol{e}}) \to 0$.

There exists an approach in control theory, known as emulation, that formally addresses the issue of discretization of a continuous time controller [18]. The related stability property addressed in emulation is that of semi-global practical asymptotic stability, in which the sampling time, T_s, is the tuning parameter:

Definition 1. *(Semi-global practical asymptotic stability) The system (2), (3) with state $\boldsymbol{\zeta} = (\boldsymbol{e}, \dot{\boldsymbol{e}})$ is semi-globally practically asymptotically stable if there exists $\beta \in \mathcal{KL}$ such that for any $\Delta, \nu \in \mathbb{R}_{>0}$ there exists $T_s^* \in \mathbb{R}_{>0}$ such that for all $T_s \in (0, T_s^*)$ the following holds:*

$$||\boldsymbol{\zeta}(t)|| \leq \beta(||\boldsymbol{\zeta}(0)||, t) + \nu, \quad \forall ||\boldsymbol{\zeta}(0)|| < \Delta \tag{4}$$

Semi-global practical asymptotic stability refers to a system in which the states asymptotically converge to a bound about the origin. The application in robotic manipulation is that the sampling time, T_s, is related to the region of attraction and ultimate bound of the states. Thus as the sampling time decreases (i.e. is "fast enough"), the system asymptotically converges to a smaller bound about the origin (i.e. the hand manipulates the object closer to the desired reference). This is aligned with the conventional assumption that the sampling time is sufficiently small, but addressed in a formal manner with proper stability guarantees. The control problem is defined as follows:

Problem 1. *Suppose Assumptions 1-6 hold. Determine a discrete-time control law that is semi-globally practically asymptotically stable with respect to $(\boldsymbol{e}, \dot{\boldsymbol{e}}) = 0$, and satisfies the no slip condition:*

$$\boldsymbol{f}^{\mathcal{C}}(t) \in F_c, \quad \forall t > 0 \tag{5}$$

III. Proposed Control

A. Task Frame Definition

The lack of object information in tactile-based blind grasping limits the definition of $\mathcal{A}$ to the on-board sensors available to the hand. A common approach to defining $\mathcal{A}$ in such a setting is adopted here from existing techniques:

$$\boldsymbol{p}_a(\boldsymbol{q}) = \bar{\boldsymbol{p}}_t(\boldsymbol{q}), \quad R_{pa}(\boldsymbol{q}) = [\boldsymbol{\rho}_x, \boldsymbol{\rho}_y, \boldsymbol{\rho}_z] \tag{6}$$

where an acceptable choice for R_{pa} is $\boldsymbol{\rho}_x = \boldsymbol{\rho}_y \times \boldsymbol{\rho}_z, \boldsymbol{\rho}_y = \frac{\boldsymbol{p}_{t_1} - \boldsymbol{p}_{t_2}}{||\boldsymbol{p}_{t_1} - \boldsymbol{p}_{t_2}||_2}, \boldsymbol{\rho}_z = \frac{(\boldsymbol{p}_{t_3} - \boldsymbol{p}_{t_1}) \times (\boldsymbol{p}_{t_2} - \boldsymbol{p}_{t_1})}{||(\boldsymbol{p}_{t_3} - \boldsymbol{p}_{t_1}) \times (\boldsymbol{p}_{t_2} - \boldsymbol{p}_{t_1})||_2}$ [5]–[7].

For practical considerations, a local parameterization of $SO(3)$ is used to define a notion of orientation error by defining $\boldsymbol{\gamma}_a \in \mathbb{R}^3$, such that $R_{pa} = R_{pa}(\boldsymbol{\gamma}_a)$ [2]. The task state is thus $\boldsymbol{x} = (\boldsymbol{p}_a, \boldsymbol{\gamma}_a)$. To incorporate this local parameterization in the kinematics, let $S(\boldsymbol{\gamma}_a) \in \mathbb{R}^{3\times3}$ denote the one-to-one mapping defined by $\boldsymbol{\omega}_a = S(\boldsymbol{\gamma}_a)\dot{\boldsymbol{\gamma}}_a$. The matrix $S(\boldsymbol{\gamma}_a)$ is absorbed into $P(\boldsymbol{x}) = \text{diag}(I_{3\times3}, S(\boldsymbol{\gamma}_a))$ such that $\begin{bmatrix} \dot{\boldsymbol{p}}_a \\ \boldsymbol{\omega}_a \end{bmatrix} = P(\boldsymbol{x})\dot{\boldsymbol{x}}$. For notation, P will be used to denote $P(\boldsymbol{x})$. A local parameterization of R_{pa} is then used to define $\boldsymbol{\gamma}_a$, one example of which is:

$$\boldsymbol{\gamma}_a(\boldsymbol{q}) = \begin{bmatrix} \arctan(-\boldsymbol{\rho}_{z_2}/\boldsymbol{\rho}_{z_3}) \\ \sqrt{1 - \boldsymbol{\rho}_{z_1}^2} \\ \arctan(-\boldsymbol{\rho}_{y_1}/\boldsymbol{\rho}_{x_1}) \end{bmatrix} \tag{7}$$

It is inherently assumed that this local parameterization is appropriately defined such that $\boldsymbol{\gamma}_a$ does not pass through a singular configuration.

B. Discrete Control

The proposed control law is derived by using emulation to combine the continuous time robust control law from [14] with grasp force optimization. The robust control law framework from [14] provides semi-global asymptotic/exponential stability about $(\boldsymbol{e}, \dot{\boldsymbol{e}}) = 0$, while compensating for uncertainties in object center of mass, object mass, external wrenches, contact locations, and hand kinematics. That control law is defined as:

$$\boldsymbol{u} = \hat{J}_h^T \Big((P^T \hat{G})^\dagger \boldsymbol{u}_m + \boldsymbol{u}_f \Big) + \hat{\boldsymbol{g}} \tag{8}$$

$$\boldsymbol{u}_m = -K_p \boldsymbol{e} - K_i \int_0^t \boldsymbol{e}\ dt - K_d \dot{\boldsymbol{e}} \tag{9}$$

where $\hat{J}_h \in \mathbb{R}^{3n \times m}$ is an estimate of the hand Jacobian, $\hat{\boldsymbol{g}} \in \mathbb{R}^m$ is an estimate of the gravity torques acting on the hand, $K_p, K_i, K_d \in \mathbb{R}^{6\times 6}$ are the respective proportional, integral, and derivative positive-definite gain matrices, and $\hat{G}$ is an approximation of the grasp map, independent of the object center of mass, defined by:

$$\hat{G} = \begin{bmatrix} I_{3\times 3}, & ..., & I_{3\times 3} \\ (\boldsymbol{p}_{c_1} - \boldsymbol{p}_a)\times, & ..., & (\boldsymbol{p}_{c_n} - \boldsymbol{p}_a)\times \end{bmatrix} \tag{10}$$

The manipulation control term, $\boldsymbol{u}_m \in \mathbb{R}^6$, determines the forces the hand must apply to manipulate the object to the reference, while rejecting disturbances from external wrenches and the uncertainties of the grasp. The internal force control term, $\boldsymbol{u}_f \in \mathbb{R}^{3n}$, determines how the hand squeezes the object to prevent slip during manipulation. The following assumptions are used for $\boldsymbol{u}_f$ and will be relaxed in Section III-C:

Assumption 7. *The internal force control satisfies:*

1) $\boldsymbol{u}_f \in Ker(G)$
2) $(\dot{\boldsymbol{x}}, \ddot{\boldsymbol{x}}) = 0 \implies \dot{\boldsymbol{u}}_f = 0$

Assumption 8. *The no slip condition (5) is satisfied.*

It is important to note that we do not assume $\hat{\boldsymbol{g}}$ exactly cancels out the gravity disturbance, nor is gravity the only external disturbance acting on the hand-object.

In following the emulation technique, a zero-order hold is applied to (8), (9) to derive the following discrete-time controller with a sampling time of T_s:

$$\boldsymbol{u}_k = \hat{J}_{h_k}^T \Big((P_k^T \hat{G}_k)^\dagger \boldsymbol{u}_{m_k} + \boldsymbol{u}_{f_k} \Big) + \hat{\boldsymbol{g}}_k \tag{11}$$

The Euler method is used to discretize $\boldsymbol{u}_m$:

$$\boldsymbol{u}_{m_k} = -K_p \boldsymbol{e}_k - K_i T_s \sum_{j=0}^{k} \boldsymbol{e}_j - \frac{K_d}{T_s}(\boldsymbol{e}_k - \boldsymbol{e}_{k-1}) \tag{12}$$

Remark 2. *A common internal force controller used in the related literature is based on the centroid position of the contacts:*

$$\boldsymbol{u}_{f_k} = K_f(\bar{\boldsymbol{p}}_{c_k} - \boldsymbol{p}_{c_{1_k}}, \bar{\boldsymbol{p}}_{c_k} - \boldsymbol{p}_{c_{2_k}}, ..., \bar{\boldsymbol{p}}_{c_k} - \boldsymbol{p}_{c_{n_k}}) \tag{13}$$

where $K_f \in \mathbb{R}_{>0}$ is a squeezing gain term [5]. Note that (13) does not guarantee the object will not slip.

Theorem 1. *Suppose Assumptions 1-8 hold. The system (2), (3) with control law (11), (12) is semi-globally practically asymptotically stable.*

Proof. The semi-global asymptotic stability of (2), (3) with control (8), (9) follows from [14], which satisfies the dissipativity property of [18]. The one-step weak consistency property from [18] is guaranteed due to the use of the Euler approximate model in (12) and the fact that the Moore-Penrose inverse can be represented as a quadratic program. Quadratic programs ensure continuity of the solution for sufficiently smoothly changes in the parameters [19], which is guaranteed from Assumptions 5 and 6. Thus the proof follows directly from Theorem 3.1 of [18]. □

C. Grasp Force Optimization and Relaxation of No Slip Assumption

The control law (11), (12) provides the desired stability guarantees, but requires the no slip assumption. Assumption 8 is relaxed here by replacing the generalized inverse and internal force controller from (11) with a grasp force optimization that is solved in-the-loop. To ensure slip does not occur, the optimization requires the direction normal to each contact point, and the assumption that the control is given a conservative estimate of μ:

Assumption 9. *There exists a lower bound, $\hat{\mu} \in \mathbb{R}_{>0}$, on the friction coefficient, μ, with associated friction cone $\hat{F}_c$.*

Tactile sensors are used to determine the contact normal direction by using knowledge of the fingertip geometry along with the measured contact location from Assumption 3. The contact frame, $\mathcal{C}_i$, is then defined by aligning one axis with the normal direction as depicted in Figure 2. The associated mapping $R_{pc_i} \in SO(3)$ rotates between contact and inertial frames. We construct $R_{pc} : \boldsymbol{f}_c^{\mathcal{C}} \mapsto \boldsymbol{f}_c^{\mathcal{P}}$ by combining each R_{pc_i} into a block diagonal matrix.

The proposed grasp force optimization is setup as a quadratic program with decision variables $\boldsymbol{z} \in \mathbb{R}^{3n}$. The decision variables represent the desired contact forces written with respect to the contact frames, $\mathcal{C}_i$. The cost function of the quadratic program is $\boldsymbol{z}^T Q_k \boldsymbol{z}$, where $Q_k := Q(\boldsymbol{q}_k, \boldsymbol{p}_{fc_k}) \in \mathbb{R}^{3n\times 3n}$ is a positive-definite, symmetric matrix. There exist numerous options for the cost function such as to minimize the internal forces: $Q_k = I_{3n\times 3n}$ or actuator torques: $Q_k = R_{pc_k}^T J_{h_k} J_{h_k}^T R_{pc_k}$ [8].

The constraints in the proposed optimization are used to ensure the contact forces manipulate the object, reside in the friction cone, and do not result in torques that saturate the motors. The manipulation constraint enforces the manipulation control term, $\boldsymbol{u}_{m_k}$, and is defined as:

$$P_k^T \hat{G}_k R_{pc_k} \boldsymbol{z} = \boldsymbol{u}_{m_k} \tag{14}$$

The friction cone constraint ensures the object does not slip. In the conventional grasp force optimization approach, the friction cone, $\hat{F}_c$, is linearized by using an inscribed l_s-faced polyhedral. The linearization results in a matrix $\Lambda(\hat{\mu}') \in \mathbb{R}^{l_s\times 3n}$, with a linearized friction coefficient, $\hat{\mu}' \in \mathbb{R}_{>0}$, where $\hat{\mu}' < \hat{\mu} \leq \mu$ [1]. Under Assumption 9, it is well known that due to the conservativeness of the linearization, the following condition is true:

$$\Lambda(\hat{\mu}') R_{pc}^T \boldsymbol{f}_c \succ 0 \implies \boldsymbol{f}_c^{\mathcal{C}} \in F_c \tag{15}$$

For a static grasp, the constraint:

$$\Lambda(\hat{\mu}') \boldsymbol{z} \succ 0 \tag{16}$$

guarantees (5) is satisfed [1], [8].

Unfortunately, (16) ignores the dynamics of the hand-object system, as well as sampling time effects, that may lead to violations of the friction condition. One potential violation is related to the effect of rolling coupled with sampling time and fingertip curvature. At time $t = kT_s$, the controller outputs a torque so that the hand applies a desired contact force on the object. During the time between $t = kT_s$ and the next sampling time $t = (k+1)T_s$, the fingertips may roll over the object, which rotates the contact normal direction. If the sampling time or fingertip curvature is too large compared to the system dynamics, the contact point may roll sufficiently far such that the constraint (16) enforced at $t = kT_s$ causes the contact force to leave the friction cone between $t = kT$ and $t = (k+1)T_s$. This phenomenon is depicted in Figure 3, with hemispherical fingertips as an example.

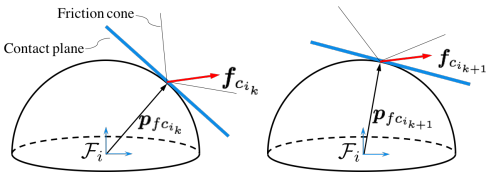

(a) $t = kT_s$ (b) $t = (k+1)T_s$

Fig. 3: The rolling of the contact plane over the fingertips between sampling times. The contact force applied at $t = kT_s$ leaves friction cone between $t = kT_s$ and $t = (k+1)T_s$.

To deal with this phenomenon, we assume there is a maximum distance the contacts may roll between sampling times. Note this assumption is valid due to the boundedness of the hand-object dynamics that will be shown in the following theorem. We use $\alpha \in \mathbb{R}$ to denote the angle between the contact point $\boldsymbol{p}_{fc_{i_k}}$ and maximum rolling distance as shown in Figure 4. Let S denote the intersection of the cone defined by α and the fingertip surface. Thus between any sampling time, the farthest the contact location may move is up to the perimeter of S. In order to satisfy all friction cones that may be encountered during the sampling period, the contact force must reside inside the intersection of all the friction cones on the perimeter of S. The intersection of all the cones forms a new friction cone defined by the effective friction coefficient, $\tilde{\mu} \in \mathbb{R}_{>0}$, where $\tilde{\mu} \leq \hat{\mu} \leq \mu$.

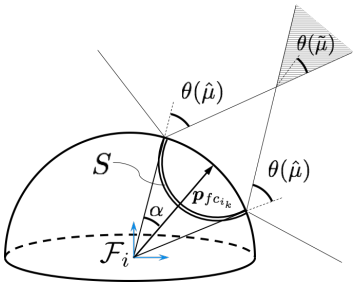

Fig. 4: The new effective friction cone, depicted as the gray region, is the intersection of all the fricion cones along the perimeter of S.

It is important to note that this issue of rolling between sampling times effectively shrinks the friction coefficient, which is equivalent to dealing with contact uncertainties in a static setting [11]. This new effective friction coefficient, $\tilde{\mu}$, can be derived as in [11] using α and knowledge of the fingertip geometry at the contact point $\boldsymbol{p}_{fc_{i_k}}$. For hemispherical fingertips, the computation is straightforward: $\tilde{\mu} = \tan(\tan^{-1}(\hat{\mu}) - \alpha)$. However the following assumption is necessary to ensure the effective friction cone exists:

Assumption 10. *The intersection of the friction cones about the perimeter of S is non-empty.*

This effective friction coefficient provides robustness to rolling, but does not handle the effect of dynamics between sampling times. In the worst case scenario, the dynamics affect the contact force in either a purely tangential or purely normal manner. An example of this is when a force disturbance acts completely tangential to a fingertip surface, and causes the object to slip. To prevent slip, the new friction cone constraint is:

$$\Lambda(\tilde{\mu}')\boldsymbol{z} \succ \varepsilon \tag{17}$$

where $\varepsilon \in \mathbb{R}_{>0}$ is a tuning parameter, and $\tilde{\mu}'$ is the linearized form of the friction coefficient $\tilde{\mu}$, such that $\tilde{\mu}' < \tilde{\mu} \leq \hat{\mu} \leq \mu$.

Finally, to prevent motor saturation, the commanded torque must be bounded between the maximum and minimum actuator torque values, $\boldsymbol{\tau}_{max}, \boldsymbol{\tau}_{min} \in \mathbb{R}^m$, respectively. This actuator constraint is:

$$\boldsymbol{\tau}_{min} < \hat{J}_{h_k}^T R_{pc_k} \boldsymbol{z} + \hat{\boldsymbol{g}}_k < \boldsymbol{\tau}_{max} \tag{18}$$

The proposed control law with grasp force optimization is formally defined by:

$$\boldsymbol{u}_k = \hat{J}_{h_k}^T R_{pc_k} \boldsymbol{z}_k^* + \hat{\boldsymbol{g}}_k \tag{19}$$

$$\begin{aligned} \boldsymbol{z}_k^* &= \underset{\boldsymbol{z}}{\operatorname{argmin}}\ \boldsymbol{z}^T Q_k \boldsymbol{z} \\ &\text{s.t.} \quad (14), (17), (18) \end{aligned} \tag{20}$$

Theorem 2. *Suppose Assumptions 1-6, 9, and 10 hold. The system (2), (3) with control law (19), (20), (12) is semi-globally practically asymptotically stable, and (5) is satisfied.*

Proof. We start by showing that slip does not occur between sampling times. The first step involves solving for $\boldsymbol{f}_c$ in (2):

$$\boldsymbol{f}_c = J_h^{-T}\Big(- M_h \ddot{\boldsymbol{q}} - C_h \dot{\boldsymbol{q}} + \boldsymbol{u}_k + \boldsymbol{\tau}_e \Big) \tag{21}$$

We substitute (19) into (21) and pre-multiply by $\Lambda(\tilde{\mu}')R_{pc}^T$. Using Assumption 9, (15) can be re-written as:

$$\Lambda(\tilde{\mu}')R_{pc}^T J_h^{-T}\Big(- M_h \ddot{\boldsymbol{q}} - C_h \dot{\boldsymbol{q}} + \hat{J}_{h_k}^T R_{pc_k} \boldsymbol{z}_k^* + \boldsymbol{\tau}_e - \hat{\boldsymbol{g}}_k \Big) \succ 0 \tag{22}$$

Solving for $\boldsymbol{z}_k^*$ results in:

$$\Lambda(\tilde{\mu}')R_{pc}^T J_h^{-T} \hat{J}_{h_k}^T R_{pc_k} \boldsymbol{z}_k^* \succ \Lambda(\tilde{\mu}')R_{pc}^T J_h^{-T}\Big(M_h \ddot{\boldsymbol{q}} + C_h \dot{\boldsymbol{q}} - \boldsymbol{\tau}_e + \hat{\boldsymbol{g}}_k \Big) \tag{23}$$

Consequently, if the proposed control satisfies (23), then (5) follows. This may be achieved by establishing existence of a

bound on the right hand side of (23), and that the left-hand side vector elements satisfy this bound.

It is clear that $\Lambda(\tilde{\mu}')$ and R_{pc}^T are bounded terms. Assumption 1 ensures that J_h^{-T} is bounded, and it is well known that there exists a uniform bound for M_h and C_h [20]. From Assumptions 5 and 6, the dynamics are smooth and so there exists a bound on $\ddot{\boldsymbol{q}}, \dot{\boldsymbol{q}}$ between sampling times. Further, the disturbance $\boldsymbol{\tau}_e$ and the gravity compensation $\hat{\boldsymbol{g}}_k$, are bounded from Assumption 6. Thus the right hand side of (23) can be conservatively bounded by $\varepsilon' \in \mathbb{R}_{>0}$:

$$\varepsilon' \succ \Lambda(\tilde{\mu}')R_{pc}^T J_h^{-T}\Big(M_h\ddot{\boldsymbol{q}} + C_h\dot{\boldsymbol{q}} - \boldsymbol{\tau}_e + \hat{\boldsymbol{g}}_k\Big) \tag{24}$$

Now we show that the left-hand side of (23) is always greater than ε'. Let $B_k = J_{h_k}^T R_{pc_k}, B = J_h^T R_{pc}$ and $B_\delta = B - B_k$, such that the left-hand side of (23), can be written as: $\Lambda(\tilde{\mu}')\Big(I_{3n\times 3n} - B^{-1}B_\delta\Big)\boldsymbol{z}_k^*$. Given any $\delta \in \mathbb{R}_{>0}$, from the boundedness and smoothness of J_h, R_{pc} and (18), there exists a sampling time, $T_1^* \in \mathbb{R}_{>0}$, such that for all $T_s \in (0, T_1^*)$, $||B^{-1}B_\delta||||\Lambda(\tilde{\mu}')||||\boldsymbol{z}_k^*|| \leq \delta$.

By choosing $\varepsilon_k > \delta + \varepsilon'$, and use of the triangle inequality, it is straightforward to satisfy (23). Finally, by Assumption 10, the use of $\tilde{\mu}'$ ensures that the contact force remains in the friction cone between sampling times. The same analysis applies to each subsequent time step up to some maximum N. Now by choosing $\varepsilon \geq \max\{\varepsilon_k : k \in (0, N)\}$, it follows that $\boldsymbol{f}_c^{\mathcal{C}} \in FC \ \forall t \in (0, NT_s)$.

By constraint (14), the proposed control outputs the same manipulation control as (11), such that the internal force component is an element of $\text{Ker}(\hat{G})$, and thus of $\text{Ker}(G)$ by Lemma 6 from [14]. When $(\dot{\boldsymbol{x}}, \ddot{\boldsymbol{x}}) = 0$, $(\dot{\boldsymbol{q}}, \ddot{\boldsymbol{q}}) = 0$ and $(\dot{\boldsymbol{x}}_o, \ddot{\boldsymbol{x}}_o) = 0$ from Lemma 3 of [14]. This implies that R_{pc}, J_h, and the internal force component are constant when $(\dot{\boldsymbol{x}}, \ddot{\boldsymbol{x}}) = 0$.

Consequently, from the same analysis as Theorem 1 and by choosing N sufficiently large, $(\boldsymbol{e}, \dot{\boldsymbol{e}})$ will converge to a ball about the origin for $t \in (0, NT_s)$. Thus it is straightforward to show that $\ddot{\boldsymbol{q}}, \dot{\boldsymbol{q}}$ are bounded in closed loop under the proposed control as $N \to \infty$ and there exists $\varepsilon = \max\{\varepsilon_k : k > 0\}$ such that semi-global practical asymptotic stability and (5) holds. Note that the maximum sampling time, $T_s^* \in \mathbb{R}_{>0}$ of the system such that semi-global practical asymptotic stability and (5) holds is: $T_s^* = \min\{T_1^*, T_2^*\}$, where $T_2^* \in \mathbb{R}_{>0}$ is the maximum allowable sampling time from the semi-global practical stability condition.

□

Remark 3. *Theorem 2 proves that the proposed control is robust to uncertainties from $\hat{J}_h, \hat{\boldsymbol{g}}$, $\hat{G}$, and assumes no knowledge of the object center of mass, object mass, or any other external wrenches acting on the hand-object. The original control from [14] and thus (11), (12) is also robust to contact location uncertainty. Contact location uncertainties cause an error in the R_{pc_k} term of the proposed control, however robustness to these uncertainties can be attained by using a more conservative friction coefficient in (20) [11].*

Remark 4. *The proposed control uses only joint angle and contact location feedback to robustly manipulate the object. One limitation of this is that the motion of the task frame defined by (6) does not exactly coincide with object motion due to the effects of rolling. This is a common problem in related work [5], [6]. However if vision sensors are available, the proposed control and stability guarantees can be readily extended to incorporate vision feedback by use of the robust manipulation framework from [14].*

IV. Simulation and Exerimental Results

A. Numerical Simulation

The simulations compare the proposed control, (19), (20), (12) with the conventional-centroid controller (11), (12),(13), and the conventional grasp force optimization control (19), (20), (12) with $\varepsilon \equiv 0$, which is denoted the conventional-gfo approach. The setup of the simulation is depicted in Figure 5, in which the Allegro Hand is grasping a rectangular prism object. A step external force is applied about the object center of mass at $t = 0.0s$, which are both unknown to the controllers. The manipulation controller is commanded to maintain the initial position and orientation such that $\boldsymbol{r} = \boldsymbol{x}(0)$. The simulation parameters are listed in Table I, and the parameters associated with the Allegro Hand can be found at http://www.simlab.co.kr/Allegro-Hand.htm. Without loss of generality, a 10x scaled model of the Allegro Hand is used for the simulations.

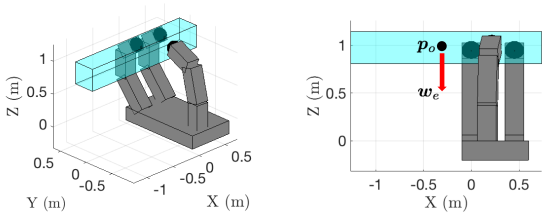

(a) (b)

Fig. 5: Simulation setup.

The simulations were performed using Matlab's ode45 integrator, with a simulation time of 15 seconds, and sampling time of $T_s = 0.003$ s. The gains, K_p, K_i, K_d in Table I were determined as in [14]. The cost function of $Q_k = R_{pc_k}^T J_{h_k} J_{h_k}^T R_{pc_k}$ was used to minimize the actuator

TABLE I: Simulation Parameters

Object dimensions	2.0 m × 0.33 m × 0.33 m
Object mass	0.05 kg
Object moment of inertia	$\text{diag}([0.0009, 0.0171, 0.0171]) \times 10^{-3}\text{kgm}^2$
Friction coefficient	$\mu, \hat{\mu}, \tilde{\mu} = 0.9,\ \tilde{\mu}' = 0.64$
Initial $\boldsymbol{p}_o$	$(-0.263, 0.041, 0.973)$ m
Initial $\boldsymbol{p}_a$	$(0.224, 0.107, 1.012)$m
Initial $\boldsymbol{\gamma}_a$	$(-0.114, 0.0, -0.565)$rad
$\boldsymbol{\tau}_e$	$-.001 * I_{m\times m}\dot{\boldsymbol{q}}$ Nm
$\boldsymbol{w}_e$	$(0, 0, -1, 0, 0, 0)$ N
K_p	$10.02 * I_{6\times 6}$
K_i	$4.00 * I_{6\times 6}$
K_d	$4.05 * I_{6\times 6}$
K_f	10.0

torques, which by Assumption 1, is guaranteed to be positive-definite. The value of K_f was determined empirically. The friction cone was linearized using a 4-sided pyramid such that $\tilde{\mu}' = \frac{\sqrt{2}}{2}\tilde{\mu}$ [8].

Figure 6 shows the position and orientation error of the system as the proposed control compensates for the external wrench applied on the object. The plots show the error converging to the origin, which is inline with the stability guaranteed by the proposed control. It is important to note that the error trajectory of both the proposed and conventional controllers are identical, as expected, due to the constraint (14) enforced in (20).

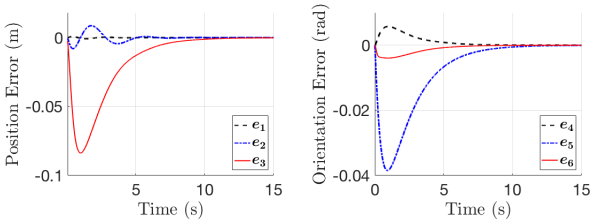

(a) Position error. (b) Orientation error.

Fig. 6: Error trajectory of proposed controller.

Figure 7 shows the "required" friction for both the conventional controllers and proposed control. The required friction, $\beta_i = \sqrt{f_{x_i}^2 + f_{y_i}^2}/f_{n_i}$, is the ratio of tangential to normal forces, and represents the friction needed so that the object does not slip. The dashed black line visually shows the true friction coefficient, μ, such that if any required friction curve exceeds μ, the object slips. We note that the simulations are not stopped if slip occurs. Figure 7 shows that the conventional-centroid control exceeds the allowable friction as the disturbance acts on the system. This is not merely due to an improper choice of K_f, but because the direction of the centroid is outside of the friction cone for contacts 1 and 2. Thus any scaling of the internal force control still causes slip, and so the conventional-centroid control is unable to grasp the object at all. Figure 7b shows that the conventional-gfo controller slips as the step disturbance acts on the system, and also between $t = 0.29$s and $t = 2.61$s as the manipulation controller drives the error to zero. Figure 7c shows that the proposed control can both manipulate the object and reject uncertain disturbances, while still ensuring the friction condition is not violated. These results motivate the analysis from Theorem 2 that defines a minimum bound on ε to guarantee no slip despite the effects of dynamics *and* sampling time. Related work that neglect these effects may be subject to slipping in such situations [11]–[13].

B. Experimental Results

In the experiment, the Allegro Hand is used to manipulate two objects to desired reference positions and orientations by means of the conventional-centroid control (11), (12), (13), and the proposed control (19), (20), (12). The two objects are a 51 gram, spherically-shaped thermos lid, and a 129 gram, flat-surfaced glasses case. The Allegro Hand setup includes

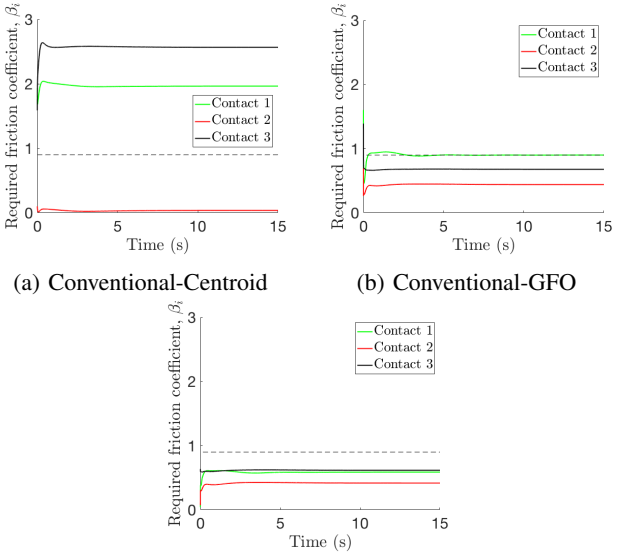

(a) Conventional-Centroid (b) Conventional-GFO

(c) Proposed, $\varepsilon = 0.3$

Fig. 7: Required friction of conventional vs proposed controllers. The dashed line indicates the friction coefficient, μ.

a NI USB-8473s High-Speed CAN. The CAN uses a fixed sampling time of $T_s = 0.003s$. The experimental setup is shown in Figure 8. Note that the Allegro Hand is equipped with force sensors, which were not used in this experiment. Approximate contact location measurements were provided to both controllers.

The gains used for the proposed and conventional-centroid controllers are listed in Table II. Note that the error bounds $v_p = 0.005$ m, $v_o = 0.07$ rad, were defined for the position and orientation errors respectively, to prevent the hunting effect that results from integral action in the presence of static friction. Thus the summation in (12) was stopped when the error satisfied: $||(\boldsymbol{e}_1, \boldsymbol{e}_2, \boldsymbol{e}_3)||_\infty \leq v_p$, $||(\boldsymbol{e}_4, \boldsymbol{e}_5, \boldsymbol{e}_6)||_\infty \leq v_o$. The controllers were given a reference command of $\boldsymbol{r} = \boldsymbol{x}(0) + \Delta\boldsymbol{r}$, where $\Delta\boldsymbol{r} = (r_x, 0, 0, 0, 0, r_\psi)$, and $r_x, r_\psi \in \mathbb{R}$ respectively denote the desired translation along the X-axis and rotation about the Z-Axis.

Figure 9 shows the position and orientation error resulting from the proposed controller manipulating the object to $r_\psi = 0.1$ radians. The plots in Figure 9 shows the orientation error converging to the prescribed error bounds, whilst the position error remains inside the error bounds. The same manipulation task was attempted using the conventional-centroid control, however due to the slipping depicted in Figure 1b, the system quickly became unstable, and the hand dropped the object.

TABLE II: Experiment Parameters

K_p	diag[(200, 200, 200, 1.15, 1.15, 1.15)]
K_i	diag[(30, 30, 30, 0.4, 0.4, 0.4)]
K_d	diag[(0.005, 0.005, 0.005, 0.05, 0.05, 0.05)]
Friction coefficient, $\tilde{\mu}$	2.5
ε	1.25
K_f	80.0

The proposed and conventional-centroid controllers were implemented with step changes of r_ψ and r_x for rota-

(a) (b)

Fig. 8: Experimental setup.

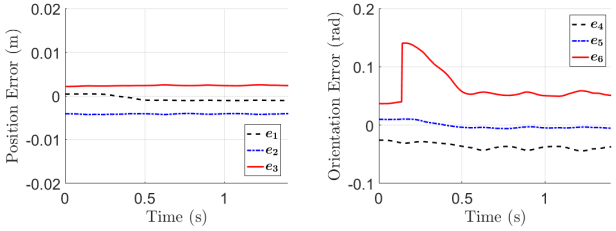

(a) (b)

Fig. 9: Position and orientation error from proposed control.

tion/Cartesian translation tasks for both objects. These results, which are included in the attached video segment, show that both the conventional-centroid and proposed controllers can manipulate the spherically-shaped object without slipping. The conventional-centroid approach slips and drops the flat-surfaced object when attempting the manipulation task. Only the proposed control was able to successfully manipulate both objects for both translation and rotation tasks. The results demonstrate how the proposed control effectively uses the available on-board information to robustly manipulate unknown objects. The conventional-centroid controller requires conservative assumptions that the object does not slip. As shown in these results, that assumption does not hold in general and limits the application of that approach.

We note that although the videos show promising results, there are signs of small slipping occurring using the proposed control. Although these do not result in system instability, they highlight the lack of analysis regarding how tactile measurement error affects the robustness of the proposed control. Future work will investigate the effect of contact location measurement errors for a more robust solution.

Another limitation of the proposed control results from conservativeness. The constraint (17) imposes a lower bound of $\varepsilon/\tilde{\mu}'$ on the contact normal force. Thus a more conservative controller (larger values of ε, smaller values of $\tilde{\mu}'$) requires larger internal contact forces and thus larger actuator torques. If the controller is too conservative, the required torques may exceed the actuator constraint (18), and impede the ability of the proposed approach to manipulate objects.

V. Conclusion

In this paper a robust discrete time control was proposed for object manipulation in tactile-based blind grasping. The proposed control was shown to be robust to grasp uncertainties, while guaranteeing that the object does not slip within the grasp. The stability analysis guarantees semi-global practical asymptotic stability of the closed loop system and accounts for the effects of sampling time. Simulation and experimental results show the effectiveness of the proposed controller. Future work will investigate how to relax the conservativeness of the approach, without compromising the stability guarantees.

References

[1] J. Kerr and B. Roth, "Analysis of multifingered hands," *The International Journal of Robotics Research*, vol. 4, no. 4, pp. 3–17, 1986.

[2] A. Cole, J. Hauser, and S. Sastry, "Kinematics and control of multi-fingered hands with rolling contact," *IEEE Transactions on Automatic Control*, vol. 34, no. 4, pp. 398–404, 1989.

[3] A. Cloutier and J. Yang, "Design, control, and sensory feedback of externally powered hand prostheses: A literature review," *Critical Reviews In Biomedical Engineering*, vol. 41, no. 2, pp. 161–181, 2013.

[4] C. Cheah, H. Han, S. Kawamura, and S. Arimoto, "Grasping and position control for multi-fingered robot hands with uncertain jacobian matrices," in *Proceedings of the IEEE International Conference on Robotics and Automation*, vol. 3, 1998, pp. 2403–2408.

[5] A. Kawamura, K. Tahara, R. Kurazume, and T. Hasegawa, "Dynamic grasping of an arbitrary polyhedral object," *Robotica*, vol. 31, no. 4, pp. 511–523, 2013.

[6] T. Wimböck, C. Ott, A. Albu-Schäffer, and G. Hirzinger, "Comparison of object-level grasp controllers for dynamic dexterous manipulation," *International Journal of Robotics Research*, vol. 31, no. 1, pp. 3–23, 2012.

[7] Z. Chen, N. Y. Lii, T. Wimböck, S. Fan, H. Liu, and A. Schäffer, "Experimental analysis on spatial and cartesian impedance control for the dexterous DLR/HIT II hand," *International Journal of Robotics and Automation*, vol. 29, no. 1, pp. 1–13, 2014.

[8] M. Nahon and J. Angeles, "Real-time force optimization in parallel kinematic chains under inequality constraints," *IEEE Transactions on Robotics and Automation*, vol. 8, no. 4, pp. 439–450, 1992.

[9] M. Buss, H. Hashimoto, and J. B. Moore, "Dextrous hand grasping force optimization," *IEEE Transactions on Robotics and Automation*, vol. 12, no. 3, pp. 406–418, 1996.

[10] L. Han, J. C. Trinkle, and Z. X. Li, "Grasp analysis as linear matrix inequality problems," *IEEE Transactions on Robotics and Automation*, vol. 16, no. 6, pp. 663–674, 2000.

[11] P. Fungtammasan and T. Watanabe, "Grasp input optimization taking contact position and object information uncertainties into consideration," *IEEE Transactions on Robotics*, vol. 28, no. 5, pp. 1170–1177, 2012.

[12] A. Caldas, A. Micaelli, M. Grossard, M. Makarov, P. Rodriguez-Ayerbe, and D. Dumur, "Object-level impedance control for dexterous manipulation with contact uncertainties using an LMI-based approach," in *Proceedings of the IEEE International Conference on Robotics and Automation*, 2015, pp. 3668–3674.

[13] Y. Fan, L. Sun, M. Zheng, W. Gao, and M. Tomizuka, "Robust dexterous manipulation under object dynamics uncertainties," in *Proceedings of the IEEE International Conference on Advanced Intelligent Mechatronics*, 2017, pp. 613–619.

[14] W. Shaw-Cortez, D. Oetomo, C. Manzie, and P. Choong, "Object manipulation using robotic hands with varying degrees of grasp knowledge," *IEEE Transactions on Robotics (under review)*, 2018.

[15] Z. Kappassov, J. A. Corrales, and V. Perdereau, "Tactile sensing in dexterous robot hands - review," *Robotics and Autonomous Systems*, vol. 74, pp. 195–220, 2015.

[16] R. Murray, Z. Li, and S. Sastry, *A mathematical introduction to robotic manipulation*. CRC Press: Boca Raton, FL, USA, 1994.

[17] K. Hang, M. Li, J. A. Stork, Y. Bekiroglu, F. T. Pokorny, A. Billard, and D. Kragic, "Hierarchical fingertip space: A unified framework for grasp planning and in-hand grasp adaptation," *IEEE Transactions on Robotics*, vol. 32, no. 4, pp. 960–972, 2016.

[18] D. S. Laila, D. Nesic, and A. R. Teel, "Open- and closed-loop dissipation inequalities under sampling and controller emulation," *European Journal of Control*, vol. 8, no. 2, pp. 109–125, 2002.

[19] J. W. Daniel, "Stability of the solution of definite quadratic programs," *Mathematical Programming*, vol. 5, no. 1, pp. 41–53, 1973.

[20] M. W. Spong, *Robot dynamics and control*. Wiley, 1989.